CHEMISTRY
A EUROPEAN JOURNAL

FULL PAPER

DOI: 10.1002/chem.201103899

Controlled Synthesis of Carbon-Encapsulated Copper Nanostructures by Using Smectite Clays as Nanotemplates

Theodoros Tsoufis,*[a] Jean-François Colomer,[b] Enrico Maccallini,[a] Lubos Jankovič,[c] Petra Rudolf,*[a] and Dimitrios Gournis[c]

Abstract: Rhomboidal and spherical metallic-copper nanostructures were encapsulated within well-formed graphitic shells by using a simple chemical method that involved the catalytic decomposition of acetylene over a copper catalyst that was supported on different smectite clays surfaces by ion-exchange. These metallic-copper nanostructures could be separated from the inorganic support and remained stable for months. The choice of the clay support influenced both the shape and the size of the synthesized Cu nanostructures. The synthesized materials and the supported catalysts from which they were produced were studied in detail by TEM and SEM, powder X-ray diffraction, thermal analysis, as well as by Raman and X-ray photoelectron spectroscopy.

Keywords: chemical vapor deposition · clays · copper · encapsulation · nanostructures

Introduction

Hybrid systems that consist of metal nanoparticles that are encapsulated within carbon nanostructures (carbon nanotubes, fullerenes, onions, etc.) form a new class of nanomaterials that exhibit very interesting physical and chemical properties that are related to their decreased dimensions. In general, the graphitic shell that surrounds the metallic core effectively prevents aggregation of the particles,[1] whilst at the same time avoiding the undesirable oxidation of the metal.[2] Furthermore, the graphitic shell can be chemically tuned upon demand to achieve self-assembly[3] of the hybrid structures into ordered arrangements. On the other hand, the size of the metal nanoparticles is closely connected to their properties[4] and their geometrical shape[5] is another critical factor in determining their behavior.[6] For nanoparticles, a different geometrical shape implies that different facets and fractions of atoms are located at the corners or edges, which affords diverse possibilities for forming defects (that result from the loss of atoms at these locations). Thus, dissimilar shapes result in differences in their properties, for example, in their catalytic behavior.[2]

[a] Dr. T. Tsoufis, Dr. E. Maccallini, Prof. Dr. P. Rudolf
Zernike Institute for Advanced Materials
University of Groningen
Nijenborgh 4, 9747AG Groningen (Netherlands)
Fax: (+31) 50-363-7208
E-mail: theodoros.tsoufis@gmail.com
p.rudolf@rug.nl

[b] Dr. J.-F. Colomer
Research Center in Physics of Matter and
Radiation (PMR), University of Namur (FUNDP)
Rue de Bruxelles 55, 5000 Namur (Belgium)

[c] Dr. L. Jankovič, Prof. Dr. D. Gournis
Department of Materials Science and Engineering
University of Ioannina, 45110 Ioannina (Greece)

Copper nanoparticles have attracted considerable attention because of their catalytic, thermal, optical, and conducting properties.[7] Copper nanoparticles can be utilized as a low-cost replacement[8] for silver and gold nanoparticles, which are currently used in the inkjet printing of conductive patterns, but have been also proposed as very efficient electrocatalysts in solid-oxide fuel cells[9] and as high-performance catalysts.[10] To date, various synthetic routes, including radiation methods,[11] microemulsion techniques,[12] supercritical techniques,[13] thermal reduction,[7] sonochemical reduction,[14] laser ablation,[15] chemical reduction,[16] metal-vapor synthesis,[17] and vapor deposition under high vacuum[7] have been employed to obtain differently shaped copper nanostructures. However, the main obstacle for using metallic-copper nanoparticles is their spontaneous oxidation under ambient conditions, particularly as their size become smaller.[18]

Herein, we elucidate the role of smectite clays as templates for the synthesis of metallic-copper nanostructures that are surrounded by multiple carbon shells by catalytic chemical vapor deposition (CCVD). The catalytic chemical vapor decomposition of hydrocarbons over Cu at high temperatures is a very promising, versatile, and reproducible method to produce different types of carbon-based nanostructures (e.g., carbon nanotubes (CNTs)[19] and graphene[20]). On the other hand, clay minerals have been reported as supports for the catalytic synthesis of graphitic structures (e.g., CNTs[21]) in the past. Owing to their unique swelling-, ion-exchange-, and intercalation properties, smectite clays can be easily, uniformly, and reproducibly loaded with metal cations, which, upon calcination, are transformed into oligonuclear metal oxides that are strongly immobilized on the layered clay surfaces. Herein, we propose a simple chemical method that involves the decomposition of acetylene over a copper-oxide catalyst that is supported on smec-

tite clay surfaces, thereby resulting in the formation of metallic-copper nanostructures that are encapsulated within graphitic shells. A natural montmorillonite clay and a synthetic hectorite (laponite) clay, which both belong to the smectite clay family, were employed as nanotemplates to evaluate the effect of the surface-charge density and platelet size of the clay mineral on the size and shape of the synthesized core–shell nanostructures. The clay was loaded with copper cations through a simple cation-exchange reaction and calcined at 450 °C to produce the corresponding copper oxides, followed by CCVD synthesis of the copper nanostructures that were encapsulated within carbon shells at 700 °C for 60 min by using acetylene as a carbon source. The products were characterized by a combination of characterization techniques, including thermogravimetric analysis (TGA), TEM and SEM, Raman and photoelectron (XPS) spectroscopy, as well as X-ray diffraction (XRD).

Results and Discussion

TEM and SEM confirmed the successful formation of metallic-copper nanoparticles that were encapsulated within graphitic shells and revealed details regarding their morphology and size. Figure 1 shows SEM images of the products after the CCVD of the two copper-exchanged clays. The sphere-like morphology of the synthesized structures could be clearly seen for the products that were grown on both supports. Nevertheless, the role of the support seems to be important for determining the size of the synthesized structures, with SWy-2 affording larger structures compared to those obtained over Laponite RD. This difference can be rationalized by considering that the amount of copper cations that are intercalated into the copper-exchanged clay catalysts is much higher in the case of SWy-2 owing to its considerably higher cation-exchange capacity (76.2 mequiv/100 g) than the corresponding value of Laponite RD (48.1 mequiv/100 g). The size difference of the produced copper nanostructures could also be influenced by the different sizes of the supporting clay platelets.

The CCVD products can be easily separated from the aluminosilicate supports by dispersing them in a polar solvent, such as EtOH. TEM measurements show the presence of isolated carbon-coated copper nanostructures after their removal from the clay support. In fact, the catalytic conversion of acetylene over Cu-exchanged SWy-2 resulted in the formation of rhomboidal structures (Figure 2a) with an average length of between 200 nm and 500 nm. Each copper rhombus is coated by well-formed, closed carbon shells (Figure 2b) with an approximate overall thickness of the order of 20 nm, as determined by HRTEM (Figure 2c).

On the other hand, TEM images revealed that the catalytic conversion of acetylene over Cu-exchanged Laponite RD resulted in quasi-spherical copper structures (Figure 3a) that were fully coated by multiple well-formed carbon shells with an outer diameter of about 200 nm. HRTEM images showed that the average thickness of the graphitic shells was about 12 nm (Figure 3b). Careful analysis of the HRTEM images suggests that the carbon shells that surround the copper core in the case of Cu-exchanged Laponite RD are more graphite-like than in the case of Cu-exchanged SWy-2. In fact, Figure 3b and the inset show the formation of multiple graphitic layers in the case of the laponite clay. On the contrary, the graphitic shells in the case of Cu-exchanged montmorillonite (Figure 2c) are barely visible and more amorphous-like, thus indicating a lower degree of graphitization. These findings are further supported by the Raman and TGA results (see below).

Figure 4 shows the XRD patterns of the Cu-exchanged clays before and after calcination at 450 °C and the synthesized clay–carbon–copper nanostructures. In the case of Cu-exchanged SWy-2 (Figure 4a), the sharp reflection at $2\theta = 7.2°$ corresponds to a basal spacing (d_{001}) of 12.3 Å, which fully agrees with the previously reported results of copper-intercalated montmorillonite, thereby confirming the successful exchange of the sodium cations of the natural clay mineral with copper cations[22] (Figure 5a).

Given that each clay layer is 9.6 Å thick, the d_{001} spacing of (12.3 ± 0.5) Å corresponds to an interlayer distance (Δ) of $12.3 - 9.6 = 2.7$ Å. After heating at 450 °C for 4.5 h, the shape

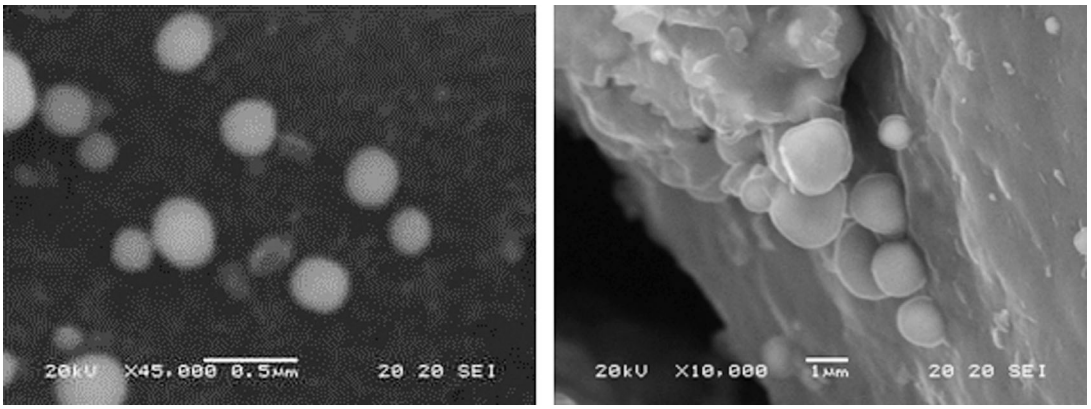

Figure 1. SEM images of copper nanostructures that are encapsulated within graphitic carbon shells; the nanostructures were synthesized by acetylene decomposition over Cu-exchanged SWy-2 montmorillonite (right) and Laponite RD (left).

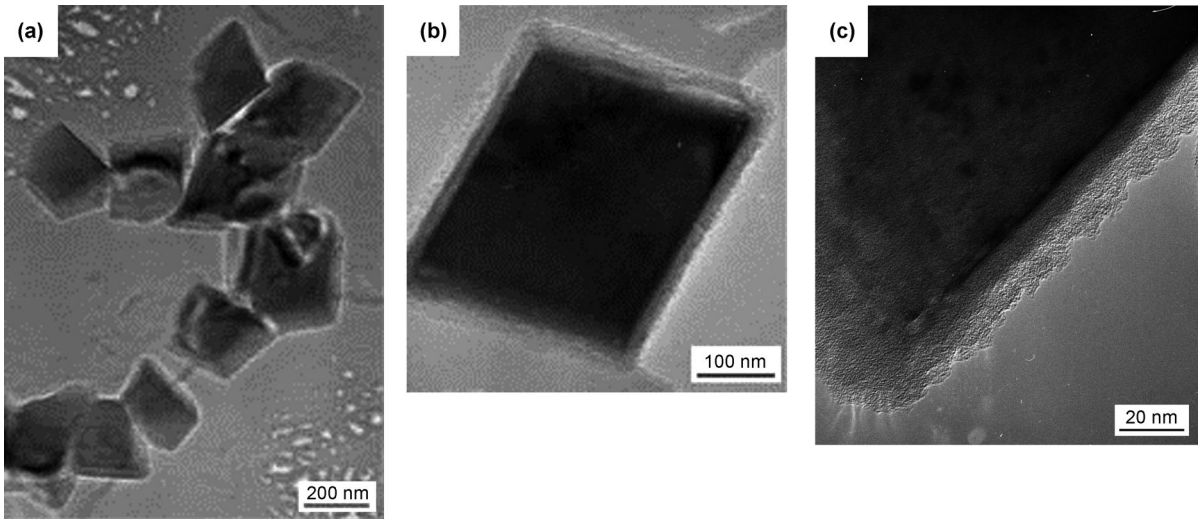

Figure 2. Low- (a) and high-magnification TEM images (b,c) of rhomboid copper nanostructures that are encapsulated within graphitic carbon shells; these shells were synthesized by acetylene decomposition over Cu-exchanged SWy-2 montmorillonite.

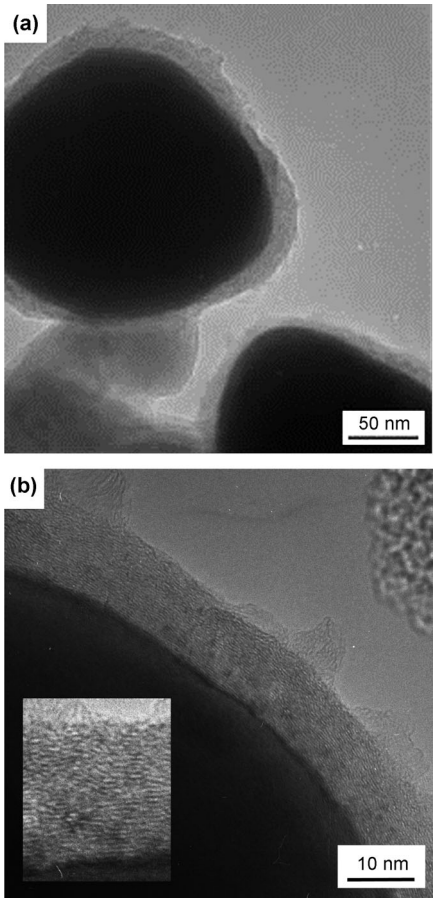

Figure 3. Low- (a) and high-magnification TEM images (b) of quasi-spherical copper spheres that are encapsulated within graphitic carbon shells; these shells were synthesized by acetylene decomposition over Cu-exchanged Laponite RD. Inset: high-resolution image that shows the graphitic layers that surround the copper spheres.

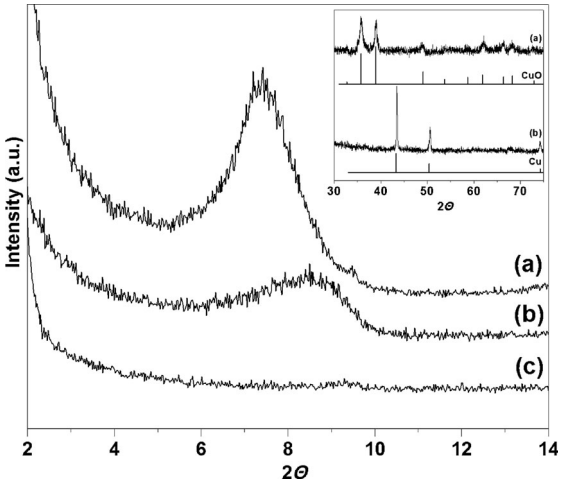

Figure 4. XRD patterns of Cu-exchanged Swy-2 montmorillonite before (a) and after calcination at 450 °C (b) and after acetylene decomposition (c). Inset: Cu-exchanged Swy-2 after calcination at 450 °C (a) and after acetylene decomposition (b). The diffraction patterns of CuO (JCPDS #74-1021) and Cu (JCPDS #04-0836) are shown for comparison.

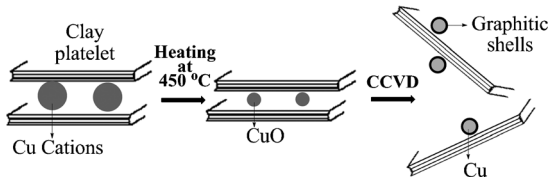

Figure 5. Schematic representation of the synthetic strategy: Starting from the Cu-exchanged clay (left), the corresponding pillared clay is produced by heating at 450 °C (middle) and the Cu nanostructures become encapsulated within graphitic carbon shells by CCVD (right).

of the 001 diffraction becomes much broader and the d_{001} spacing decreases dramatically to 9.9 Å (Figure 4b), thus suggesting the complete dehydration of the interlayer copper cation (Figure 5b) and the subsequent formation of copper oxide (CuO). This result was further indicated by

the appearance of a new set of diffraction peaks at $2\theta =$ 39.1°, 48.8°, 66.3°, and 68.3°, which are characteristic of CuO (Figure 4, inset a). The catalytic decomposition of acetylene at 700 °C over the formed copper oxides that were supported on SWy-2 resulted in the formation of the metallic-copper, as indicated by the appearance of characteristic peaks at 43.5° (a (111) reflection) and 50.5° (a (200) reflection; Figure 4, inset b). Moreover, the lack of strong reflections at low angles (Figure 4c) implies that most of the montmorillonite layers are delaminated after CCVD (Figure 5c).

Cu-exchanged Laponite RD shows a rather broad 001 diffraction peak (Figure 6a) owing to the low aspect ratio of laponite[23] clay. Thus, the d_{001} spacing was calculated with relatively lower accuracy to be about (12.2 ± 1.5) Å, which corresponds to $\Delta = 2.6$ Å. This interlayer distance is almost identical to that calculated for Cu-exchanged SWy-2. Calcination of the copper-exchanged laponite resulted in a shift of the 001 diffraction peak to higher 2θ values, thereby suggesting the collapse of the interlayer space owing to dehydration of the intercalated copper cations and the subsequent formation of copper oxide. Also, in this case, the formation of the oxide phase was further confirmed by the appearance of the characteristic set of copper oxide diffraction peaks at higher 2θ values (Figure 6, inset a). The catalytic decomposition of acetylene transformed the latter phase that was supported on laponite into metallic copper (Figure 6, inset b); this process also resulted in the loss of structural order, as indicated by the absence of any strong reflections at low 2θ angles (Figure 6c).

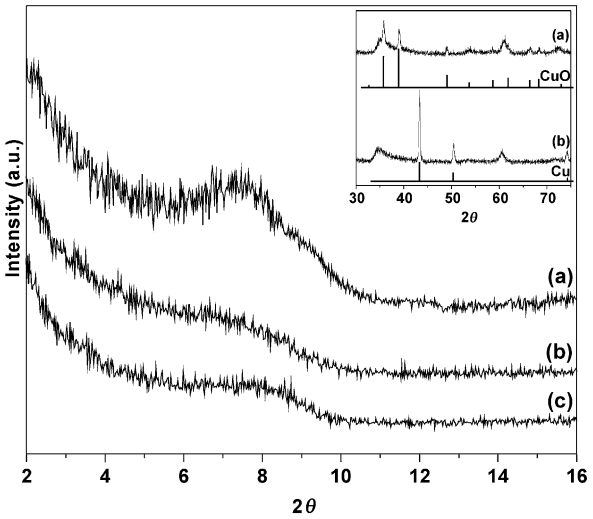

Figure 6. XRD patterns of the Cu-exchanged Laponite RD before (a) and after calcination at 450 °C (b) and after acetylene decomposition (c). Inset: Copper-exchanged laponite after calcination at 450 °C (a) and after acetylene decomposition (b). The diffraction patterns of CuO (JCPDS #74-1021) and Cu (JCPDS #04-0836) are shown for comparison.

The chemical state of copper in the synthesized nanostructures was further studied by XPS. For the copper nanostructures that were synthesized over both clay minerals, the spectra (Figure 7, left) showed a single doublet peak in which the Cu $2p_{3/2}$ was centered at a binding energy of

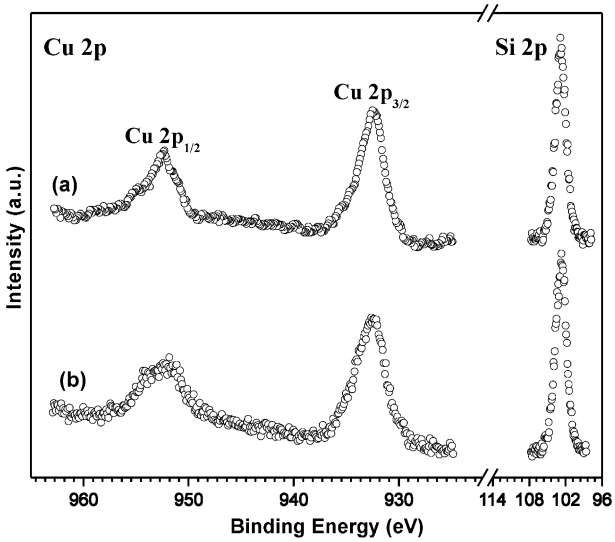

Figure 7. Cu 2p and Si 2p core-level XPS spectra of carbon-coated copper nanostructures that were synthesized by decomposition of acetylene over Cu-exchanged SWy-2 (a) and Laponite RD (b).

932.7 eV; this value was in agreement with previously reported values for Cu^{1+} or metallic Cu species[24] (Cu^{2+} species are reported at binding energies well-above 933 eV[25]). This finding, together with the absence of satellite structures on the high-binding-energy side of the Cu $2p_{3/2}$ peak, was in agreement with the XRD results, excluding the presence of CuO after the CCVD growth. In fact, shake-up satellites cannot occur in metallic Cu nor in Cu^{1+} compounds owing to their completely filled 3d shells.[25c]

XPS can not only provide qualitative but also quantitative information[26] because the peak area of an element (normalized by the corresponding atom-sensitivity factor and the transmission of the analyzer) is proportional to the amount of corresponding atoms within the sampling depth. In this sense, the relative peak-area ratio of Si 2p (Figure 7, right), which originated from the inorganic skeleton of the clay and was recorded at 102.8 eV,[23] to Cu $2p_{3/2}$ could be used to estimate the total amount of carbon-coated copper nanostructures on the clay platelets. The relative Si/Cu ratio was higher in the case of laponite (10.9) than for SWy-2 (9.7), thus implying that the higher CEC of the natural clay is also responsible for the relatively higher percentage of copper that was present in the synthesized structures after CCVD.

A very powerful method for the characterization of the quality of the carbon-coating is Raman spectroscopy.[27] Two characteristic peaks at about 1300 and 1600 cm^{-1}, which corresponded to the graphite D- and G bands, respectively, were present in the Raman spectra of all of the synthesized carbon-coated copper nanostructures (Figure 8). The

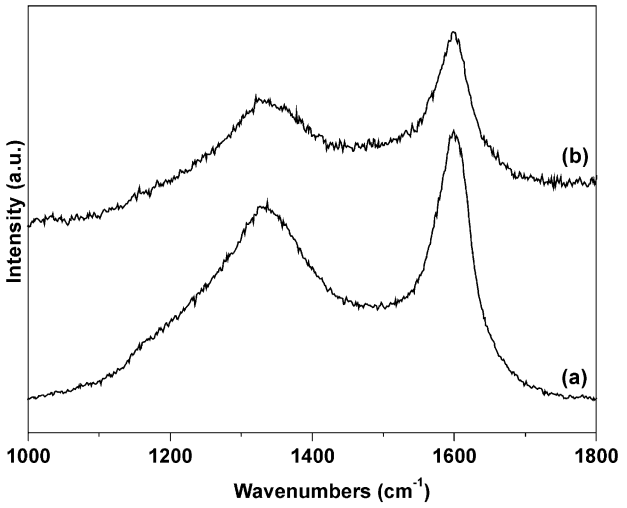

Figure 8. Raman spectra of carbon-coated copper nanostructures that were synthesized by acetylene decomposition over Cu-exchanged SWy-2 montmorillonite (a) and Cu-exchanged Laponite RD (b).

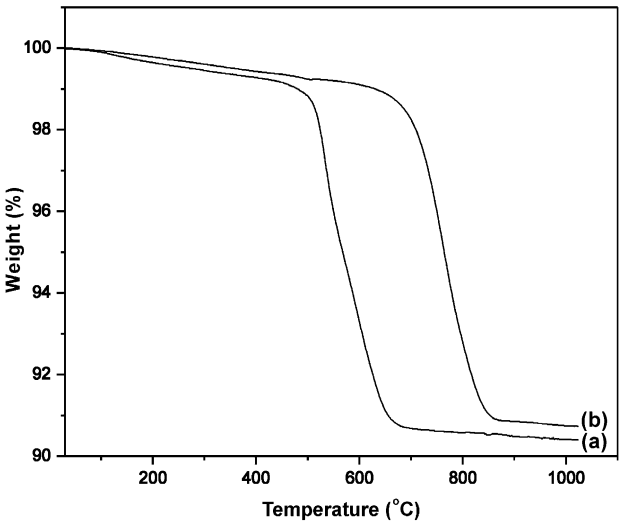

Figure 9. TGA of carbon-coated Cu nanostructures that were synthesized by decomposition of acetylene over copper oxide that was supported on SWy-2 montmorillonite (a) and Laponite RD (b).

G band corresponds to the tangential stretching (E_{2g}) mode of highly oriented pyrolytic graphite (HOPG) and can be used to assess the degree of crystallinity/graphitization, whilst the D band (at lower wavenumbers) originates from disorder in the sp^2-hybridized carbon atoms and is characteristic of lattice distortions in curved graphene sheets.[28] The intensity ratio of the D and G bands (I_D/I_G) reveals the degree of disorder in the graphite sheets and can be used as a measure of the crystallinity—and thus the quality—of the synthesized graphitic structures.[29] I_D/I_G was found to be 0.76 in the case of the nanostructures that were synthesized on SWy-2 and 0.70 when Laponite RD was used as the support. Both of these values suggest that the graphitic shells that surround the metallic-copper nanostructures show a high degree of graphitization and that the laponite-supported copper oxides result in better formed graphitic shells than their corresponding montmorillonite-supported copper oxides. Nevertheless, the presence of a number of point-like defects (pentagon-/heptagon-shaped carbon rings, sp^3-hybridized atoms, and vacancies) cannot be excluded and has been reported for similar-shaped graphitic structures.[30]

TGA was used to determine the percentage of deposited carbon and, subsequently, the percentage of the graphitic shells in the synthesized materials (Figure 9). In general, two major weight losses are recorded when heating the samples in air: the first one occurs at around 300–400 °C and corresponds to the removal of amorphous carbon by dry oxidation, whilst the second one, typically above 400 °C, stems from burning graphitic carbon structures. The amount of graphitic carbon per catalyst (Graph/cat. wt. %) can be estimated according to the formula $(\Delta W^{400-800})/W^{800}$, where $\Delta W^{400-800}$ is the weight loss between 400 and 800 °C and W^{800} is the remaining sample weight at 800 °C.[29b,31] The amount of graphitic carbon per catalyst for the materials that were produced by using copper-exchanged montmorillonite and laponite were 8.7 and 8.3 %, respectively. These calculated values suggest that the activity of the clay-supported copper-oxide catalysts in producing graphitic structures is not greatly influenced by the type of clay support (montmorillonite or laponite). However, significant weight-loss commences just above 500 °C for the nanostructures that are produced on SWy-2, whilst for those that are grown on Laponite RD, it only starts at temperatures well-above 650 °C. Taking into account that the presence of numerous defects in the graphitic layers is considered to lower their relative thermal stability, thereby providing edges and dangling bonds for oxidative combustion,[32] and that higher oxidation temperatures are very often associated with less-defective graphitic nanostructures, these findings support the conclusions from Raman spectroscopy and TEM analysis that, in the case of CCVD on Cu-exchanged calcined Laponite RD, stable graphitic shells are produced with better quality and/or structural organization than when SWy-2 is used as the support.

Conclusion

In conclusion, we have described the successful synthesis of stable metallic copper nanostructures inside graphitic onions by the CCVD of acetylene over clay-supported copper oxide catalysts. These results showed that the choice of the clay support greatly affected the shape and size of the final nanostructures. The use of natural clay (SWy-2 montmorillonite) as the support promotes the formation of rhomboidal structures that are larger in size than the corresponding spherical structures that are synthesized when synthetic clay (Laponite RD) acts as catalyst support. This trend is attributed to the different cation-exchange capacities and platelet sizes of the clays: Montmorillonite has a considerably higher cation-exchange capacity compared to laponite, thereby re-

sulting in a denser packing of the copper cations in the interlayer space. Thus, because in CCVD the size of the catalyst is closely related to the resulting size of the synthesized graphitic structures,[33] the metallic-copper particles in the case of montmorillonite are larger in size.

Experimental Section

A natural and a synthetic clay of the smectite group with different charge-layer densities were used in this work. The natural clay was a Wyoming montmorillonite (SWy-2) that was obtained from the Source Clay Minerals Repository at the University of Missouri, Columbia. Prior to use, it was fractionated to $<2\,\mu m$ by gravity sedimentation and purified according to well-established procedures in clay science.[34] Sodium-exchanged samples were prepared by immersing the clay in 1 M sodium chloride. Cation exchange was completed by washing and centrifuging four times with a dilute aqueous solution of NaCl. Finally, the samples were washed with distilled-deionized water and transferred into dialysis tubes to obtain chloride-free clays and dried at RT. The cation-exchange capacity (CEC) of SWy-2 was 76.4 mequiv per 100 g and an average platelet size of 200 nm. The synthetic clay was a commercial trioctahedral hectorite (Laponite RD) that was produced by Laporte Industries Ltd.; the synthetic clay was used as received with a CEC of 48.1 mequiv per 100 g clay and an average platelet size of 20 nm. The copper-cation-exchanged samples of SWy-2 and Laponite RD were prepared by the multiple overnight saturation of clay suspensions with 1 mol dm^{-3} $CuCl_2$ solutions, washed well with distilled water, separated by centrifugation, dried at 60 °C, ground to pass through a 0.2 mm sieve, and finally calcined at 450 °C in air for 4.5 h. The synthesis of the graphitic-carbon-encapsulated copper nanostructures was carried out by the catalytic decomposition of acetylene (Linde, 99.9 %) over clay-supported copper oxides in a fixed-bed flow reactor at a temperature of 700 °C. In detail, the clay-copper powder (about 100 mg) was placed in an alumina boat within a quartz tube (inner diameter: 2.2 cm and length: 90 cm) that was located in the central region of a resistance furnace. Each catalyst was heated to 700 °C under a nitrogen atmosphere. At this temperature, acetylene as a carbon precursor was mixed with the carrier gas (N_2) at flow rates of 10 $cm^3 min^{-1}$ and 90 $cm^3 min^{-1}$, respectively. After 60 min, the C_2H_2 gas flow was stopped and the ceramic boat was left to cool to RT under a nitrogen atmosphere. The synthesized material was collected from the ceramic boat as a black powder.

TEM was performed on a JEOL 200CX microscope working at 200 kV. A few milligrams of each material were dispersed in EtOH and one droplet was added onto a holey carbon grid, left to dry, and examined. SEM images were recorded on a JEOL JSM-5600 V scanning electron microscope. The TEM and SEM images are typical and representative of the samples in question. X-ray powder diffraction data were collected on a D8 Advance Bruker diffractometer by using $Cu_{K\alpha}$ (40 kV, 40 mA) radiation and a secondary beam graphite monochromator. The patterns were recorded in the range $2\theta = 2$–$80°$ in steps of 0.02° and a counting time of 2 s per step. For the X-ray photoemission measurements, the samples were introduced by using a load-lock system into a SSX-100 (Surface Science Instruments) photoelectron spectrometer with a monochromatic $Al_{K\alpha}$ X-ray source ($h\nu = 1486.6$ eV). The base pressure in the spectrometer was 3×10^{-10} Torr and the energy resolution was set to 1.16 eV to minimize measuring time. The photoelectron take-off angle was 37° and an electron-flood gun, in combination with a gold grid that was placed above the sample surface, was used to compensate for sample charging. Evaporated Au(111) films that were prepared by vacuum sublimation (10^{-7} mbar) of gold (99,99 %, Umicore Materials AG) onto freshly cleaved mica sheets that were preheated at 375 °C in a custom-built evaporator were used as substrates. The samples were dispersed in water and, after short stirring time, a small drop of the suspension was drop-cast onto the substrate and left to dry at RT. The binding energies were referenced to the Si 2p binding energy of the clay silicon (102.8 eV).[35] Spectroscopic analysis included a Shirley background subtraction and peak separation by using mixed Gaussian–Lorentzian functions in a least-squares curve-fitting program (Winspec) that was developed at the University of Namur, Belgium. Quantitative analysis that was based on the photoemission peak areas was performed by taking into account the sensitivity factors for each element, which were specific to the spectrometer used. Raman spectra were recorded at 532 nm (Nd-YAG) by using a Renishaw RM 1000 Micro-Raman system. A power of 0.5–1 mW was focused onto a 1 μm spot to avoid the photodecomposition of the samples. Typically, the Raman spectra were recorded with 4 to 5 exposures of 5–10 s duration. Further analysis of the Raman spectra involved manual baseline correction where appropriate. TGA was performed on a Shimadzu stand-alone Thermal Analyzer. The samples (about 5 mg) were heated in a stream of air (40 mL min^{-1}) at a rate of 5 °C min^{-1}. Highly sintered α-Al_2O_3 was used as a thermally inert reference material.

Acknowledgements

J.F.C. is supported by the FRS-FNRS (Belgium) as a Research Associate. This work received financial support from the "Stichting voor Fundamenteel Onderzoek der Materie (FOM)", which is financially supported by the "Nederlandse Organisatie voor Wetenschappelijk Onderzoek (NWO)".

[1] S. Seraphin, D. Zhou, J. Jiao, *J. Appl. Phys.* **1996**, *80*, 2097–2104.
[2] L. Jankovič, D. Gournis, P. N. Trikalitis, I. Arfaoui, T. Cren, P. Rudolf, M. H. Sage, T. T. M. Palstra, B. Kooi, J. De Hosson, M. A. Karakassides, K. Dimos, A. Moukarika, T. Bakas, *Nano Lett.* **2006**, *6*, 1131–1135.
[3] A. B. Dongil, B. Bachiller-Baeza, A. Guerrero-Ruiz, I. Rodríguez-Ramos, A. Martínez-Alonso, J. M. D. Tascón, *J. Colloid Interface Sci.* **2005**, *281-292*, 179–189.
[4] a) M. A. El-Sayed, *Acc. Chem. Res.* **2004**, *37*, 326–333; b) R. H. Kodama, *J. Magn. Magn. Mater.* **1999**, *200*, 359–372.
[5] a) Y. Sun, Y. Xia, *Science* **2002**, *298*, 2176–2179; b) K. L. Kelly, E. Coronado, L. L. Zhao, G. C. Schatz, *J. Phys. Chem. B* **2003**, *107*, 668–677.
[6] C. Burda, X. Chen, R. Narayanan, M. A. El-Sayed, *Chem. Rev.* **2005**, *105*, 1025–1102.
[7] a) H. H. Huang, F. Q. Yan, Y. M. Kek, C. H. Chew, G. Q. Xu, W. Ji, P. S. Oh, S. H. Tang, *Langmuir* **1997**, *13*, 172–175; b) J. A. Eastman, S. U. S. Choi, S. Li, W. Yu, L. J. Thompson, *Appl. Phys. Lett.* **2001**, *78*, 718–720; c) N. A. Dhas, C. P. Raj, A. Gedanken, *Chem. Mater.* **1998**, *10*, 1446–1452.
[8] M. Grouchko, A. Kamyshny, S. Magdassi, *J. Mater. Chem.* **2009**, *19*, 3057–3062.
[9] a) S. Park, R. J. Gorte, J. M. Vohs, *Appl. Catal. A* **2000**, *200*, 55–61; b) Y. Wang, A. V. Biradar, G. Wang, K. K. Sharma, C. T. Duncan, S. Rangan, T. Asefa, *Chem. Eur. J.* **2010**, *16*, 10735–10743.
[10] S. Vukojević, O. Trapp, J. Grunwaldt, C. Kiener, F. Schüth, *Angew. Chem.* **2005**, *117*, 8192–8195; *Angew. Chem. Int. Ed.* **2005**, *44*, 7978–7981.
[11] N. A. Koratkar, J. Suhr, A. Joshi, R. S. Kane, L. S. Schadler, P. M. Ajayan, S. Bartolucci, *Appl. Phys. Lett.* **2005**, *87*, art. no.063102.
[12] M. P. Pileni, B. W. Ninham, T. Gulik-Krzywicki, J. Tanori, I. Lisiecki, A. Filankembo, *Adv. Mater.* **1999**, *11*, 1358–1362.
[13] H. Ohde, F. Hunt, C. M. Wai, *Chem. Mater.* **2001**, *13*, 4130–4135.
[14] C. N. R. Rao, B. C. Satishkumar, A. Govindaraj, M. Nath, *ChemPhysChem* **2001**, *2*, 78–105.
[15] M. S. Yeh, Y. S. Yang, Y. P. Lee, H. F. Lee, Y. H. Yeh, C. S. Yeh, *J. Phys. Chem. B* **1999**, *103*, 6851–6857.
[16] S. H. Wu, D. H. Chen, *J. Colloid Interface Sci.* **2004**, *273*, 165–169.
[17] G. Vitulli, M. Bernini, S. Bertozzi, E. Pitzalis, P. Salvadori, S. Coluccia, G. Martra, *Chem. Mater.* **2002**, *14*, 1183–1186.
[18] S. Gangopadhyay, G. C. Hadjipanayis, B. Dale, C. M. Sorensen, K. J. Klabunde, V. Papaefthymiou, A. Kostikas, *Phys. Rev. B* **1992**, *45*, 9778–9787.

[19] a) D. Takagi, Y. Homma, H. Hibino, S. Suzuki, Y. Kobayashi, *Nano Lett.* **2006**, *6*, 2642–2645; b) L. F. Su, J. N. Wang, F. Yu, Z. M. Sheng, *Chem. Vapor Depos.* **2005**, *11*, 351–354.
[20] A. Reina, X. Jia, J. Ho, D. Nezich, H. Son, V. Bulovic, M. S. Dresselhaus, K. Jing, *Nano Lett.* **2009**, *9*, 30–35.
[21] D. Gournis, M. A. Karakassides, T. Bakas, N. Boukos, D. Petridis, *Carbon* **2002**, *40*, 2641–2646.
[22] C. Mosser, L. J. Michot, F. Villieras, M. Romeo, *Clay Miner.* **1997**, *45*, 789–802.
[23] D. Gournis, L. Jankovic, E. Maccallini, D. Benne, P. Rudolf, J. F. Colomer, C. Sooambar, V. Georgakilas, M. Prato, M. Fanti, F. Zerbetto, G. H. Sarova, D. M. Guldi, *J. Am. Chem. Soc.* **2006**, *128*, 6154–6163.
[24] a) R. J. Bird, P. Swift, *J. Electron Spectrosc. Relat. Phenom.* **1980**, *21*, 227–240; b) J. G. Jolley, G. G. Geesey, M. R. Hankins, R. B. Wright, P. L. Wichlacz, *Appl. Surf. Sci.* **1989**, *37*, 469–480; c) J. P. Espinós, J. Morales, A. Barranco, A. Caballero, J. P. Holgado, A. R. Gonzalez-Elipe, *J. Phys. Chem. B* **2002**, *106*, 6921–6929.
[25] a) J. H. Moulder, W. F. Stickle, P. E. Sobol, K. D. Bomben, Handbook of X-ray Photoelectron Spectroscopy, Physical Electronics, Inc. USA, **1995**; b) B. R. Strohmeier, D. E. Levden, R. S. Field, D. M. Hercules, *J. Catal.* **1985**, *94*, 514–530; c) T. H. Fleisch, G. J. Mains, *Appl. Surf. Sci.* **1982**, *10*, 51–62.
[26] D. Briggs, M. P. Seah, in *Practical Surface Analysis*, Wiley, Chichester **1990**.
[27] a) T. Tsoufis, A. Tomou, D. Gournis, A. P. Douvalis, I. Panagiotopoulos, B. Kooi, V. Georgakilas, I. Arfaoui, T. Bakas, *J. Nanosci. Nanotechnol.* **2008**, *8*, 5942–5951; b) T. Tsoufis, L. Jankovic, D. Gournis, P. N. Trikalitis, T. Bakas, *Mater. Sci. Eng. B* **2008**, *152*, 44–49.
[28] a) P. C. Eklund, J. M. Holden, R. A. Jishi, *Carbon* **1995**, *33*, 959; b) V. Georgakilas, D. Gournis, M. A. Karakassides, A. Bakandritsos, D. Petridis, *Carbon* **2004**, *42*, 865–870.
[29] a) I. V. Pavlidis, T. Tsoufis, A. Enotiadis, D. Gournis, H. Stamatis, *Adv. Eng. Mater.* **2010**, *12*, B179–183; b) E. Maccallini, T. Tsoufis, A. Policicchio, S. La Rosa, T. Caruso, G. Chiarello, E. Colavita, V. Formoso, D. Gournis, R. G. Agostino, *Carbon* **2010**, *48*, 3434–3445.
[30] S. Tomita, M. Fujii, S. Hayashi, *Phys. Rev. B* **2002**, *66*, 2454241–2454247.
[31] T. Tsoufis, P. Xidas, L. Jankovic, D. Gournis, A. Saranti, T. Bakas, M. A. Karakassides, *Diam. Relat. Mater.* **2007**, *16*, 155–160.
[32] D. Bom, R. Andrews, D. Jacques, J. Anthony, B. Chen, M. S. Meier, J. P. Selegue, *Nano Lett.* **2002**, *2*, 615–619.
[33] a) H. Dai, A. G. Rinzler, P. Nikolaev, A. Thess, D. T. Colbert, R. E. Smalley, *Chem. Phys. Lett.* **1996**, *260*, 471–475; b) T. Yamada, T. Namai, K. Hata, D. N. Futaba, K. Mizuno, J. Fan, *Nat. Nano* **2006**, *1*, 131–136.
[34] D. Gournis, V. Georgakilas, M. A. Karakassides, T. Bakas, K. Kordatos, M. Prato, M. Fanti, F. Zerbetto, *J. Am. Chem. Soc.* **2004**, *126*, 8561–8568.
[35] T. Ebina, T. Iwasaki, A. Chatterjee, M. Katagiri, G. D. Stucky, *J. Phys. Chem. B* **1997**, *101*, 1125–1129.

Received: December 12, 2011
Revised: March 26, 2012
Published online: June 20, 2012

